

# DESIGN AND DEVELOPMENT OF CURCUMIN LOADED CHIA SEED MUCILAGE BASED ELECTROSPRAYED NANOPARTICLES: *IN VITRO-EX VIVO* CHARACTERIZATION

SWAPNIL V. THAKARE and ASHISH P. GORLE

*Department of Pharmaceutics, R. C. Patel Institute of Pharmaceutical Education and Research, Shirpur,  
Maharashtra 425 405, India*

✉ *Corresponding author: A. P. Gorle, ashishgorle@rediffmail.com*

*Received November 15, 2023*

Chia seed mucilage (CSM) has recently been reported as a biocompatible polymeric matrix for drug delivery. Curcumin (CUR), an active phytoconstituent widely recognized for managing colon and other types of cancer, faces limitations, such as poor water solubility and low bioavailability. Hence, this study focuses on developing CUR-loaded CSM-based electrospayed nanoparticles (ENPs) using the electrospaying technology. The particle size and zeta potential of the optimized batch (F9) were measured at 82.20 nm and 22.39 mV, respectively. Solubility studies confirmed that the optimized CUR-ENPs exhibit higher solubility compared to bare CUR, with a 92.25% drug release in 12 h (pH 5.8). The designed CUR-ENPs showed good biocompatibility in normal FHC-CRL-1831 cell lines over the bare CUR. Moreover, CUR-ENPs demonstrated a reduction in % cell viability in the preferred HCT116 cell line as a colorectal cancer cell line over bare CUR. In conclusion, the designed electrospayed CUR-ENPs demonstrate improved solubility of CUR.

**Keywords:** curcumin, chia seed mucilage, electrospaying, nanoparticles, anticancer activity

## INTRODUCTION

Colorectal cancer ranks as the third most prevalent and the second most deleterious neoplastic burden.<sup>1</sup> Global records for 2020 reveal an alarming tally of 1.9 million documented cases, resulting in 0.9 million fatalities. Projections anticipate a surge to 3.2 million instances by 2040.<sup>2</sup> Primarily, surgical interventions constitute the primary modality for addressing colorectal cancer.<sup>3</sup> Unfortunately, a disconcerting trend emerges, wherein over fifty percent of cancer patients manifest recurrence and metastasis post-resection.<sup>4,5</sup> Current data underscore chemotherapy and radiation as the foremost therapeutic avenues for combating this malignancy.<sup>6</sup> In the chemotherapy domain, exploration into irinotecan, oxaliplatin, and capecitabine has yielded promising outcomes in clinical applications targeting colorectal cancer.<sup>7</sup> Nevertheless, the irrefutable emergence of drug resistance and consequential harm to normal tissues has punctuated the efficacy of these pharmaceutical interventions.<sup>8,9</sup> Despite their intrinsic utility, both chemotherapy and radiation

therapies confront a plethora of limitations that necessitate attentive study before endorsing them as efficacious cancer treatment modalities.<sup>10</sup> In summation, conventional approaches exhibit circumscribed therapeutic efficacy, primarily due to inherent constraints, such as non-selectivity, dose-dependent toxicity, and resistance propensities, among other impediments.<sup>6,10</sup> The imperative to develop alternatives that transcend the limitations of established cancer treatment protocols resonates strongly in the quest for more efficacious therapeutic strategies.

Recently, there has been a documented inclination towards phytoconstituents in cancer research, attributed to their notable anticancer potential and low toxicity to normal cells.<sup>11</sup> Among the various anticancer phytoconstituents, curcumin (CUR) has garnered prolonged recognition as a naturally derived medicinal agent with inherent potential for mitigating an array of health concerns, notably including cancer.<sup>12,13</sup> Its multifaceted influence extends to the regulation of cell cycle dynamics, immune responses,

apoptosis, and various mechanisms intricately linked to the genesis and progression of tumors. Despite the pronounced therapeutic merits associated with CUR, a litany of challenges persist, encompassing factors such as limited water solubility, constrained bioavailability, rapid metabolic turnover, abbreviated biological half-life, and expeditious systemic clearance.<sup>14,15</sup> These particulars restrict the full realization of their therapeutic potential in the treatment of diverse diseases and disorders.<sup>12,14</sup> In response to these impediments, a spectrum of delivery systems has been meticulously documented to enhance the effective deployment of CUR. These encompass, but are not confined to, liposomes, nanoemulsions, nanofibers, nanogels, micelles, nanosuspensions, nanocomposites, nanoparticles, and various other carriers.<sup>16</sup> Hence, this diverse array of carriers aims to tackle the significant challenges posed by the inherent limitations of CUR, thereby enhancing its utility and efficacy in therapeutic applications.

The preference for nanotechnology is evident in its capacity to address challenges associated with phytoconstituents, including solubility, dissolution rate, bioavailability, and more.<sup>17</sup> The preference for polymeric nanoparticles for the delivery of anticancer drugs has been widely reported.<sup>18</sup> However, the techniques used for the design of polymeric nanoparticles suffer from several issues, including the use of non-degradable surfactants, high-temperature requirements, scale issues, low promise to design small particles, poor polydispersity, *etc.* Hence, there is a need to use a suitable method that can overcome the above-mentioned issues.<sup>18</sup> Electrospraying is the technique widely reported for the design of electrosprayed nanoparticles for the delivery of drug molecules. With the help of an electric field, the droplets of the drug polymeric mixture get converted into nanosized solid particles termed electrosprayed particles.<sup>18-20</sup> To date, electrosprayed nanoparticles (ENPs) have been reported for the delivery of docetaxel,<sup>21</sup> hydroxycamptothecin,<sup>22</sup> paclitaxel,<sup>23</sup> *etc.* This technique offers several merits, including high loading efficiency, optimized particle size within nanometers, and simplistic and continuous synthesis.<sup>18,19</sup> As well, it has been used for the delivery of low-soluble anticancer drug molecules.<sup>24,25</sup> Hence, the solubility of poorly soluble drugs can be enhanced via the incorporation of drug molecules, such as resveratrol, into the polymeric matrix and then the

design of ENPs via the electrospraying technique.<sup>26</sup>

Chia seeds, scientifically known as *Salvia hispanica* L., have gained global acclaim for their nutritional and functional properties.<sup>27</sup> Upon contact with water, chia seeds undergo a hydration process, forming a mucilage, similarly to other plants, algae, and microorganisms.<sup>28</sup> This process leads to the formation of a hydrogel network, regulated by hydrophilic functional groups connected to the polysaccharide's polymeric structure.<sup>29</sup> Key components of chia seed mucilage (CSM) encompass xylose, glucose, and methyl glucuronic acid, forming a highly branched polysaccharide.<sup>30</sup> Recognizing its potential, the Food and Agricultural Organization (FAO) labeled CSM in 1996 as a promising source of polysaccharide gum due to its exceptional ability to form a viscous solution in water, even at remarkably low concentrations.<sup>31</sup> Consequently, CSM stands out as a valuable source of polysaccharides for crafting polymers used in biomedical applications.<sup>32</sup> Therefore, we intend to use the electrospraying technology to improve the solubility and drug release pattern of CUR via designing CUR-loaded CSM-based electrosprayed nanoparticles (CUR-ENPs).

In this study, CUR-loaded CSM-based electrosprayed nanoparticles were fabricated using the electrospraying technique to enhance solubility and tailor the release pattern. The optimization of CUR-ENPs was carried out using the 3<sup>2</sup> (three level-two factors) response surface methodology. These nanoparticles were synthesized under optimized electrospraying parameters. The effects of independent variables, namely, the quantity of CUR (X<sub>1</sub>) and the concentration of CSM (X<sub>2</sub>), – on dependent variables, such as solubility (Y<sub>1</sub>) and drug release (Y<sub>2</sub>), were investigated using the same 3<sup>2</sup> response surface methodology. Various analyses, including Fourier-transform infrared spectroscopy (FT-IR), differential scanning calorimetry (DSC), X-ray diffractometry (XRD), particle size, polydispersity index (PDI) and zeta potential assessments, were conducted. Subsequently, a cell viability study was performed to verify the biocompatibility with normal cells and evaluate the anticancer activity against colorectal cancer cell lines. In conclusion, the designed CUR-ENPs represent a novel dosage form that could significantly enhance the solubility of poorly soluble phytoconstituents and synthetic hydrophobic drug molecules.

## EXPERIMENTAL

### Materials

CUR was procured from Sigma Aldrich, Germany, and isopropyl alcohol was sourced from Merck, India. The isolation of chia seed mucilage (CSM) was done in the laboratory using the reported method. All chemicals utilized in the study were of analytical-grade quality.

### Methods

#### Isolation of CSM from chia seeds

In this phase, chia seeds underwent meticulous washing to extract the mucilage, eliminating impurities. Cleaned seeds were stirred in a 50:1 water ratio at  $69 \pm 1$  °C, pH 8, for 12 h. The solution was filtered, and then centrifuged at 6000 rpm for 10 min at 25 °C, separating the mucilage from residual particles. The resulting mucilage was dried at 38 °C, ground, sieved, and stored in a cool, dry environment.<sup>33</sup>

#### Optimization of CUR-ENPs using response surface methodology

The statistical experimental investigation was conducted using Design-Expert software (Stat-Ease Inc., Minneapolis). The application of factorial design experiments to determine the relative significance of various components in a formulation proves to be a valuable tool. Utilizing the  $3^2$  (three-level, two factors) response surface methodology allowed for the optimization and evaluation of the influence of independent variables on responses.<sup>34</sup> Herein, the quantity of CUR ( $X_1$ ) and the quantity of CSM ( $x_2$ ) were selected as independent variables and were modified at three levels: low (-1), medium (0), and high (+1). Solubility in  $\mu\text{g/L}$  ( $Y_1$ ) and % drug release ( $Y_2$ ) were chosen as dependent parameters. Table 1 illustrates the statistical design for the selected dependent and independent variables. The following equation was employed to depict the effect of independent variables ( $X_1/x_2$ ) on dependent variables  $Y_1/Y_2$  for optimization:

$$Y = \beta_0 + \beta_1 x_1 + \beta_2 x_2 + \beta_3 x_1 x_2 + \beta_4 x_1^2 + \beta_5 x_2^2 \quad (1)$$

where the response variable is denoted as  $Y$ , with the intercept represented by  $\beta_0$ , and the regression coefficients are expressed as  $\beta_1\beta_5$ . The individual impacts are attributed to  $X_1$  and  $x_2$ . Additionally, the interaction effects are indicated by  $X_1^2$ ,  $x_2$  and the quadratic effects are represented as  $X_1^2$ ,  $x_2^2$ . The significance of the model was assessed using one-way ANOVA at a  $P$ -value  $< 0.05$  level.

#### Preparation of electrosprayed CUR-ENPs

In this study, CUR-ENPs were prepared using the electrospraying technique.<sup>35,36</sup> A total of 13 batches were produced according to the specifications outlined in Table 1 by Design Expert 11 software. The formulation involved combining CUR and CSM in 50 mL of water, which was then stirred for 30 min at 500 rpm. It was also subjected to bath sonication for 5 min

at room temperature. Subsequently, this solution underwent electrospraying using an electrospinning unit. The prepared polymeric solution was loaded into a syringe and the process was executed under optimized parameters, including a flow rate of 5 mL/h, a voltage of 20 kV, a collector drum speed set at 500 rpm, a distance of 12 cm between the collector and syringe nozzles, and a spinneret speed of 70 cycles. Upon completion of the electrospraying process, the collected CUR-ENPs underwent various characterizations, such as spectral analysis, particle size measurement, and other relevant assessments. The same methodology was consistently applied across all batches outlined in Table 1.

#### Saturation solubility study

In this procedural stage, the experiment involved the utilization of individual conical flasks, each containing 20 mL of three distinct solutions: distilled water, 0.1 N HCl, and phosphate buffer at pH 6.8.<sup>37,38</sup> Each flask served as a controlled environment for the experiment. Within each of these flasks, 10 mg of both pure CUR and an equivalent amount of CUR-ENPs were separately added. The mixtures underwent a sonication process at room temperature for 10 min to ensure proper dispersion. Following sonication, the flasks were then placed in an orbital shaking incubator set at 37 °C, utilizing equipment from Remi, India. This incubation period spanned 24 h and was carefully regulated under controlled conditions. Upon completion of the incubation phase, 5 mL aliquots of the samples were collected from each flask and subjected to filtration using Whatman filter paper to isolate the liquid phase. Subsequently, the concentration of CUR in the filtrate was quantified using an Ultraviolet-Visible (UV-Vis) Spectrophotometer (U-2900, Hitachi, Japan) at a wavelength of 426 nm. This analytical approach facilitated the accurate measurement of CUR concentration, providing essential data for evaluating the release profile of both pure CUR and CUR-ENPs under specified experimental conditions.

#### Fourier transform infrared spectroscopy (FTIR)

The interaction between CUR and CSM was examined using FTIR to determine potential relevant interactions.<sup>38</sup> In short, the FTIR spectra of pure CUR, CSM, and CUR-ENPs were recorded within the wavelength range of 4000 to 400  $\text{cm}^{-1}$ . Spectrum analysis was employed to ascertain the compatibility of the substances within the formulations. Samples were formulated in a 1:10 ratio with potassium bromide (KBr) and then scanned against a blank KBr disc, utilizing a resolution of 1  $\text{cm}^{-1}$ .

#### X-ray diffraction (XRD) analysis

The nature of plain CUR, CSM, and CUR-ENPs, whether in crystalline or amorphous form, was evaluated using an X-ray diffractometer (Bruker, D8

Advanced, Germany), employing CuK radiation (40 kV, 20 mA). The samples were analyzed using a step-scan mode of  $0.03 \text{ s}^{-1}$  across the  $2\theta$  angles in the range of  $4^\circ$ – $80^\circ$  to determine their structural characteristics.<sup>38</sup>

#### **Differential scanning calorimetry (DSC)**

The DSC (DSC-60, Shimadzu & 821, Mettler Toledo) was employed to analyze the thermal behaviors of the samples (CUR, CSM, and CUR-ENPs). Each sample, weighing 5-10 mg, was enclosed in an aluminum pan and subjected to temperature scanning from  $30^\circ\text{C}$  to  $200^\circ\text{C}$  at a heating rate of  $10^\circ\text{C}/\text{min}$ . The experiment was conducted under a nitrogen gas flow of  $80 \text{ mL}/\text{min}$ . Using the provided software, the thermal parameters of the samples, including melting points, and enthalpies of endothermic and exothermic reactions, were determined.<sup>39</sup>

#### **Particle size distribution, polydispersity index, and zeta potential analysis**

The particle sizes of the prepared curcumin-loaded engineered nanoparticles (CUR-ENPs) were meticulously assessed using the Malvern Zetasizer Model, ZS 200. A specialized particle size analyzer was employed to examine not only the particle size, but also the polydispersity index (PDI) of the CUR-ENPs. This comprehensive analysis provides insights into the uniformity and distribution of particle sizes within the formulation. Furthermore, the zeta potential, a key parameter indicative of the surface charge of the nanoparticles, was evaluated using the Malvern Zetasizer. To facilitate this assessment, samples were appropriately diluted in water at a tenfold ratio, ensuring accurate measurement and representation of the zeta potential of the CUR-ENPs. This dual-pronged approach in particle size and zeta potential analysis using advanced instrumentation contributes to a thorough characterization of the CUR-ENPs, essential for understanding their physicochemical properties and potential applications.<sup>38</sup>

#### **Scanning electron microscopy (SEM)**

The scanning electron microscopy (SEM) analysis of the optimized batch of CUR-ENPs was performed using an SEM apparatus, specifically the Jeol 6390LA, in conjunction with the Oxford XMX N system. The prepared CUR-ENPs were meticulously applied onto a specially prepared stub and subsequently subjected to a gold-coating process under conditions of high vacuum using an evaporator. The SEM analysis was conducted with precision, employing optimized voltage and pressure settings to ensure accurate imaging and detailed observations. Various magnifications were utilized during the analysis to capture the intricacies of the nanostructure, providing a comprehensive understanding of the surface morphology of the optimized batch of CUR-ENPs. This methodological approach guarantees a thorough examination of the

nano-sized features and structural characteristics, contributing to a comprehensive evaluation of the CUR-ENPs formulation.<sup>39</sup>

#### **Percentage entrapment efficiency (% EE) and drug content (% DC)**

The analysis of encapsulation efficiency (% EE) was conducted following a standardized procedure. Initially, 10 mg of CUR-ENPs was dissolved in 50 mL of water and subjected to sonication for 30 min. Subsequently, the resulting dispersion underwent centrifugation at 15,000 rpm for 30 min, and the supernatant was collected for the assessment of the % EE of CUR within the CUR-ENPs formulation. Concurrently, the determination of the drug loading efficiency (% DC) followed a similar process. In this phase, 10 mg of CUR-ENPs was dissolved in 50 mL of water, subjected to a 30-min sonication, and then centrifuged at 15,000 rpm for 30 min. The supernatant obtained from this process was utilized to evaluate the % DC of CUR in CUR-ENPs. The % DC was calculated by establishing the ratio of the amount of CUR found in the prepared CUR-ENPs to the total combined weight of curcumin and CSM. This comprehensive methodology ensures a reliable and standardized assessment of both % EE and % DC in the CUR-ENPs formulation.<sup>38,39</sup>

#### **In-vitro drug release studies**

The dissolution tests for CUR-ENPs and plain CUR were conducted using the dialysis bag method at  $37^\circ\text{C}$  at 100 rpm, employing 100 mL of phosphate buffer pH 5.8 as the dissolution media.<sup>40</sup> For each test, 50 mg of plain CUR and an equivalent amount of CUR-ENPs were dissolved in 5 mL of dissolution medium and then enclosed in a dialysis bag. Samples were periodically filtered at predetermined intervals, with an addition of 5 mL of the fresh medium after each 5 mL sample collection to maintain sink conditions. The filtered samples were then analyzed using a UV-Vis spectrophotometer at 426 nm. The obtained data were fitted into various mathematical models including zero-order, first-order, Higuchi matrix, Peppas's, and Hixson Crowell models, to understand the release kinetics and mechanism of the dosage form. The model with the best fit was selected based on the  $R^2$  values obtained. For instance, in zero-order kinetics, the equation representing drug dissolution from CUR-ENPs, assuming constant surface area and no equilibrium conditions, is the following:

$$Q_t = Q_0 + K_0 t \quad (2)$$

where  $Q_t$  represents the amount of drug dissolved at a time ' $t$ ',  $Q_0$  is the initial concentration of the drug in the solution, and  $K_0$  signifies the zero-order release constant.

For first-order kinetics, the release rate data were fitted to the following equation:

$$\text{Log } Q_t = \text{log } Q_0 + K_1 t / 2.303 \quad (3)$$

where  $Q_t$  denotes the amount of drug released at a time 't',  $Q_0$  represents the initial concentration, and  $K_1$  stands for the first-order release constant.

Higuchi introduced various theoretical models to analyze the release of water-soluble and poorly soluble medications in solid or semisolid matrices. The model intended to describe drug particles dispersed within a uniform matrix, acting as the diffusion medium, is based on the formula displayed below:

$$Q_t = K_H \cdot t^{1/2} \quad (4)$$

For Korsmeyer and Peppas's release model, the release rate data are adjusted to the equation:

$$M_t / M_\infty = K \cdot t^n \quad (5)$$

where  $M_t/M_\infty$  represents the fraction of drug release, 'K' is a constant, 't' signifies the time for release, and 'n' stands for the diffusional exponent related to the drug release, which depends on the shape of the matrix dosage form.

As for the Hixson-Crowell model, the release rate data are fitted to the equation:

$$W_0^{1/3} - W_t^{1/3} = K_s t \quad (6)$$

where ' $W_0$ ' represents the initial amount of CUR-ENPs, ' $W_t$ ' is the remaining amount of the drug in the pharmaceutical dosage form, and ' $K_s$ ' is a constant incorporating the surface-volume relation.

### Cell viability study

In this study, we employed a previously established methodology to evaluate the cytotoxicity of newly developed nanocarriers.<sup>41</sup> To assess the biocompatibility of both CUR and CUR-ENPs, we conducted experiments on different cell lines, incorporating slight modifications for optimal results. The investigation commenced by gauging the impact on normal cell lines, specifically FHC-CRL-1831 (fetal human colon epithelial cells). These cells, procured from the American Tissue Culture Collection (ATCC), were cultured and maintained in a 25 cm<sup>2</sup> flask using DMEM: F12 Medium (ATCC 30-2006). DMSO served as the positive control in this phase.

Concurrently, the cytotoxicity assessments were extended to colorectal cancer cell lines, HCT116 (human colorectal cancer cells), also sourced from ATCC. The HCT116 cell lines were cultured and maintained in a 25 cm<sup>2</sup> flask using RPMI 1640 medium and F-12K medium. The cells were meticulously handled in a sterile environment, and the cell mixture underwent centrifugation to isolate the pellet. Subsequently, the pellets were reconstituted in media and transferred to culture flasks for further incubation.

Cell counting was performed using a hemocytometer, and selected cells ( $1 \times 10^4$  cells/mL) were incubated in a CO<sub>2</sub> incubator for 24 h at 37 °C. Following this, the cells were seeded in tissue culture-grade microplates (96 wells) at a density of 104 cells/well in 100 µL of culture media. Various concentrations of CUR and CUR-ENPs (ranging from 20 µg/mL to 1200 µg/mL) were applied to assess their

cytotoxic effects. As a positive control for the colorectal cancer cell lines, 5-Fluorouracil was included. The cultures were incubated for an additional 24 h, after which MTT reagent (20 µL of 5 mg/mL) was added. The treated cells were incubated for 4 h, resulting in the formation of purple formazan crystals. After confirming the presence of crystals, the absorbance of the wells was measured at 570 nm by adding 200 µL of DMSO to the solution. Finally, the cell viability of CUR and CUR-ENPs was assessed against FHC-CRL-1831 and HCT116 cell lines to validate their biocompatibility and anticancer potential, respectively. This comprehensive approach provides insights into the potential therapeutic applications of the developed nanocarriers.

## RESULTS AND DISCUSSION

### Optimization of CUR-ENPs

The response surface methodology (RSM) employed in our study utilizes mathematical and statistical techniques to efficiently optimize experimental conditions, minimizing the need for extensive repetitions. In our investigation, we implemented a 3<sup>2</sup>-run statistical design for optimization. To comprehend the effects of independent variables, 2D plots (Fig. 1A and B) and 3D counterplots (Fig. 1C and D) were generated. The independent factors were the amounts of CUR and hydrophilic CSM, denoted as X<sub>1</sub> and X<sub>2</sub>, respectively. Solubility (µg/L) and drug release (%) were selected as the dependent variables for analysis.

Table 1 outlines the experimental runs at three levels, illustrating a solubility range of 92.5 µg/L to 128.50 µg/L. Notably, the saturation solubility of pure CUR in various media was approximately 28.11 µg/L in distilled water, 33.60 µg/L in 0.1 N HCl (pH 1.2), and 39.25 µg/L in pH 7.4 phosphate buffer. All 13 batches of CUR-ENPs demonstrated solubility within the range from 92.5 µg/L to 128.50 µg/L, showcasing significantly higher solubility than plain CUR. The concentration of hydrophilic CSM demonstrated a clear impact on the solubility of CUR, indicating a proportional relationship where an increase in the concentration of CSM correlated with enhanced solubility.<sup>38</sup> Conversely, a low concentration of CSM coupled with a high concentration of CUR led to a reduction in solubility. Therefore, the optimization of CSM is crucial in the design of electrosprayed nanoparticles loaded with CUR.

In terms of drug release, CUR-ENPs exhibited a range from 85.45% to 94.25%. Specifically, in pH 7.4 phosphate buffer, CUR-ENPs released

85.45% to 94.25% of their drugs within 12 min, signifying a considerably faster release compared to pure CUR, which released only 42.85% in the same time frame (refer to Fig. 2). This highlights that CUR-ENPs exhibit a notably enhanced drug dissolution rate compared to pure CUR. In summary, the concentration of CSM and CUR plays a significant role in influencing the release profile of CUR from CUR-ENPs.

To further assess drug release kinetics, the obtained data were fitted to kinetic models, and the patterns and mechanisms of drug release for all 13 batches are outlined in Table 2. Here, it is confirmed that the designed CUR-ENPs formulation (F9) offers zero-order ( $R^2 = 0.976$ ) release of CUR. Polynomial equations and counterplots, indicative of the effects of independent variables, were employed to analyze

the experimental data. The quadratic model of responses indicated a good fit, with correlation coefficients ( $R^2$ ) of 0.88 for solubility ( $Y_1$ ) and 0.80 for drug release ( $Y_2$ ), as detailed in Table 3. This underscores the reliability of the established mathematical models in predicting and optimizing the critical parameters influencing the solubility and drug release of CUR-ENPs in our experimental setup.

The equations for solubility ( $Y_1$ ) and drug release ( $Y_2$ ) are as follows:

$$Y_1 = +119.98 - 6.86x_1 + 9.04x_2 - 9.24x_1^2 + 1.63x_2^2 + 8.40x_1x_2 \dots (7)$$

$$Y_2 = +90.44 - 0.27x_1 - 0.12x_2 - 4.22x_1^2 + 0.82x_2^2 + 2.69x_1x_2 \dots (8)$$

A positive value in the equations indicates a synergistic effect, while a negative value denotes an antagonistic effect.

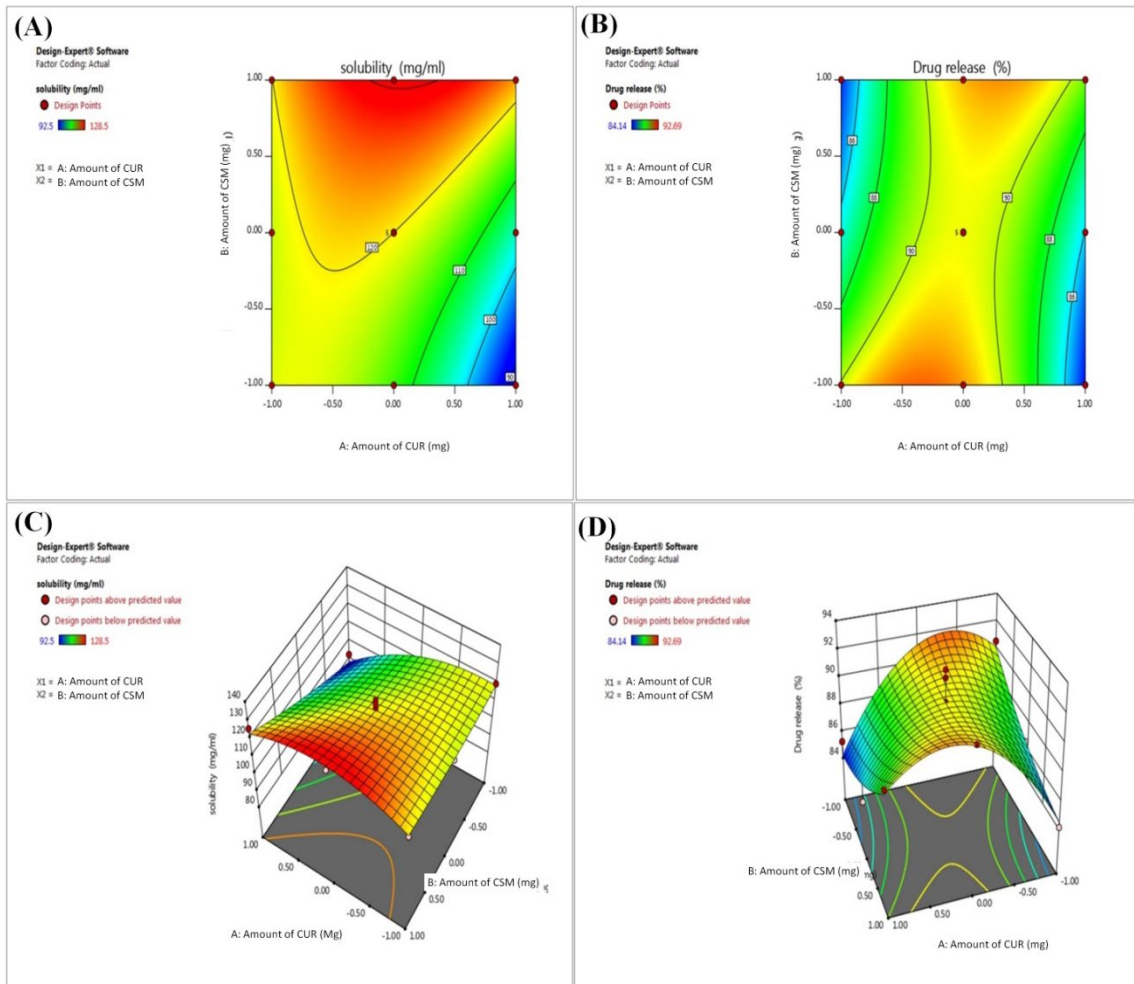


Figure 1: Contour plots for (A) solubility and (B) drug release; 3D response surface plots for (C) solubility and (D) drug release

Table 1  
Formulation composition for CUR-ENPs using  $3^2$  response surface methodology

Experimental run	Independent variable		Dependent variables	
	Amount of CUR ( $X_1$ )	Amount of CSM ( $X_2$ )	Solubility ( $Y_1$ , $\mu\text{g/L}$ )	Drug release ( $Y_2$ , %)
F1	0	0	123.5	92.69
F2	0	0	118.5	90.48
F3	0	0	121.01	88.01
F4	1	-1	92.5	85.25
F5	0	-1	107.17	89.92
F6	-1	-1	119.59	90.55
F7	1	1	125.74	89.61
F8	-1	0	117.24	86.44
F9	0	1	128.5	91.25
F10	-1	1	119.25	84.14
F11	1	0	96.69	84.65
F12	0	0	118.87	90.25
F13	0	0	125.6	92.15

Coded levels			
Independent variable	Low level (-1)	Medium level (0)	High level (+1)
$X_1$ = Amount of CUR	200	400	600
$X_2$ = Amount of CSM	200	400	600

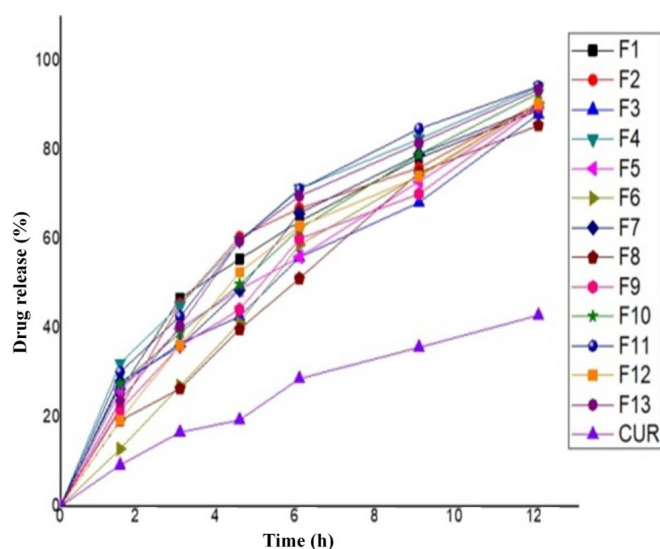


Figure 2: Dissolution profiles for pure CUR and all 13 batches of prepared optimized CUR-ENPs formulations

Table 2  
*In vitro* release kinetic for CUR-ENPs

Kinetics	F1	F2	F3	F4	F5	F6	F7	F8	F9	F10	F11	F12	F13
Zero-order	0.983	0.957	0.968	0.985	0.972	0.997	0.981	0.997	0.976	0.988	0.938	0.990	0.976
First order	0.871	0.924	0.831	0.902	0.847	0.895	0.930	0.885	0.957	0.913	0.991	0.908	0.949
Higuchi	0.962	0.985	0.916	0.932	0.944	0.976	0.964	0.974	0.966	0.972	0.990	0.991	0.997
Korsmeyer-Peppas	0.977	0.973	0.939	0.957	0.973	0.999	0.963	0.999	0.965	0.990	0.990	0.996	0.995

Table 3  
Summary of results of regression analysis for responses  $Y_1$  and  $Y_2$

Source	Std. Dev.	R-squared	Adjusted R-squared	Predicted R-Squared	PRESS	Remarks
Response solubility						
Linear	8.318111	0.527474	0.432969	-0.00497	1471.554	Suggested
2FI	6.749531	0.719995	0.62666	0.41517	856.3548	
Quadratic	4.823441	0.888779	0.809335	0.2784	1056.624	
Cubic	4.89694	0.918117	0.80348	-5.61823	9690.929	
Response % DR						
Linear	3.15262	0.005243	-0.19371	-1.00211	200.0385	Suggested
2FI	2.796662	0.295475	0.060633	-0.73949	173.7997	
Quadratic	1.658522	0.807285	0.669632	0.310979	68.84279	
Cubic	1.801906	0.837517	0.610041	-2.32185	331.8986	

Table 4 displays the ANOVA results of the model for  $Y_1$  and  $Y_2$ . The quadratic equation for solubility ( $Y_1$ ) suggests that it is influenced by independent variables, such as  $X_1X_2$ ,  $X_2^1$ ,  $X_2^2$ , and  $X_1X_2$ . Similarly, the equation for drug release ( $Y_2$ ) indicates its dependence on independent variables, including  $X_1$ ,  $X_2$ ,  $X_1^2$ ,  $X_2^2$ , and  $X_1X_2$ . The influence of these independent variables on particle size and solubility proved to be significant at a P-value <0.05. Both models displayed significance with F-values of 11.18 and 16.13 at P <0.05. Table 5 exhibits the diagnostic case statistics for various response variables, including actual, predicted, and residual values. The prediction error, derived by comparing experimental values to predicted values, revealed a small difference between actual and predicted values, indicating a well-fitted model.

**% EE and % DC**

The high % EE of  $86.22 \pm 2.2\%$  suggests that a substantial proportion of CUR was successfully encapsulated within the electrospayed nanoparticles (F9). This is a crucial parameter, as it signifies the efficiency of the formulation process in trapping and retaining the active pharmaceutical ingredient. The technique’s ability to encapsulate a high percentage of CUR reflects its proficiency in utilizing the hydrophilic polymeric matrix of CSM to entrap the drug effectively. The % DC of  $42.88 \pm 1.52\%$  further corroborates the effective loading of CUR into the ENPs. % DC represents the ratio of the amount of CUR present in the electrospayed formulation to the total combined weight of the drug and the carrier material.

Table 4  
ANOVA of models for  $Y_1$  and  $Y_2$

Source	Sum of Squares	DF	Mean Square	F Value	Prob > F	Remarks
Response Y1						
Model	1301.42	5	260.284	11.18751	0.0031	Significant
X1	282.2204	1	282.2204	12.13038	0.0102	
X2	490.1488	1	490.1488	21.06755	0.0025	
X1 <sub>2</sub>	235.6552	1	235.6552	10.12892	0.0154	
X2 <sup>2</sup>	7.364519	1	7.364519	0.316541	0.5912	
X1 X2	281.9041	1	281.9041	12.11679	0.0103	
Response Y2						
Model	80.65904	5	16.13181	5.864628	0.0191	Significant
X1	0.4374	1	0.4374	0.159014	0.7019	
X2	0.0864	1	0.0864	0.03141	0.8643	
X1 <sup>2</sup>	49.14492	1	49.14492	17.86636	0.0039	
X2 <sup>2</sup>	1.864922	1	1.864922	0.677982	0.4374	
X1 X2	28.99823	1	28.99823	10.54214	0.0141	

Table 5  
Diagnostics case statistics for various response variables

Std. order	Actual value	Predicted value	Residual	Std. order	Actual value	Predicted value	Residual
Response Y1				Response Y2			
F1	119.59	118.5943	0.99569	F1	90.55	90.12974	0.420259
F2	107.17	112.578	-5.40805	F2	89.92	91.38552	-1.46552
F3	92.5	88.08764	4.412356	F3	85.25	84.20474	1.045259
F4	117.24	117.6047	-0.36471	F4	86.44	86.49552	-0.05552
F5	121.01	119.9834	1.026552	F5	88.01	90.44379	-2.43379
F6	96.69	103.888	-7.19805	F6	84.65	85.95552	-1.30552
F7	119.25	119.881	-0.63098	F7	84.14	84.50474	-0.36474
F8	128.5	130.6547	-2.15471	F8	91.25	91.14552	0.104483
F9	125.74	122.9543	2.78569	F9	89.61	89.34974	0.260259
F10	118.87	119.9834	-1.11345	F10	90.25	90.44379	-0.19379
F11	125.6	119.9834	5.616552	F11	92.15	90.44379	1.706207
F12	118.5	119.9834	-1.48345	F12	90.48	90.44379	0.036207
F13	123.5	119.9834	3.516552	F13	92.69	90.44379	2.246207

The reported % DC indicates that a substantial portion of the CUR-ENPs is composed of CUR, contributing to the overall drug content in the ENPs. Here, electrospraying offers advantages such as precise control over particle size, enhanced drug encapsulation, and the ability to produce nanoparticles with a high surface area.

The hydrophilic nature of CSM likely contributes to the efficient entrapment of CUR during the electrospraying process, creating a stable and effective drug delivery system. In summary, the reported high % EE and % DC values in the optimized batch of electrosprayed CUR-ENPs indicate a successful formulation process. The electrospraying technique, coupled with the hydrophilic polymeric matrix of CSM, plays a pivotal role in achieving effective curcumin encapsulation, paving the way for the development of a promising drug delivery system with enhanced encapsulation and loading efficiencies.<sup>18</sup>

### DSC analysis

The primary aim of this experiment was to explore the interactions between the drug molecule (CUR) and the carriers, particularly CSM, within the formulated CUR-ENPs (F9). The investigation utilized DSC to analyze the thermal behavior of pure CUR, CSM, and the formulated CUR-ENPs. The DSC thermogram of pure CUR exhibited a prominent endothermic peak at 194.2 °C, indicating the melting point of the crystalline CUR.<sup>42</sup> CSM displayed a single endothermic peak at 58 °C, consistent with the polymer's known melting temperature. In the

thermogram of CUR-ENPs, a notable change in the endothermic peaks of both CUR and CSM was observed. The wide endothermic peak observed for CUR at 195°C in the CUR-ENPs thermogram suggests interactions between CUR and CSM within the formulated nanoparticles. The alteration in the endothermic peaks indicates a modification in the thermal behavior, indicative of molecular interactions between the drug and the polymer in the CUR-ENPs.<sup>14</sup> Importantly, this alteration in the thermal profile confirms the reduction of the crystalline nature of CUR, implying a transition into an amorphous form within the CUR-ENPs. The observed changes in the DSC thermograms strongly imply the existence of interactions between CUR and CSM within the formulated CUR-ENPs. The wide endothermic peak for CUR in CUR-ENPs, as opposed to the sharp peak in pure CUR, suggests a disruption in the crystalline structure of curcumin. This disruption can be attributed to the incorporation of CUR into the hydrophilic polymeric matrix of CSM during the formulation process. The conversion of CUR into an amorphous form is a significant finding, as amorphous drugs often exhibit improved solubility and dissolution rates, which are favorable for enhanced bioavailability. In summary, the DSC analysis provides valuable insights into the molecular interactions and changes in the crystalline nature of curcumin when formulated into CUR-ENPs with CSM. The experiment confirms the successful incorporation of CUR into the polymeric matrix, paving the way for potential improvements in drug delivery

characteristics, such as solubility and

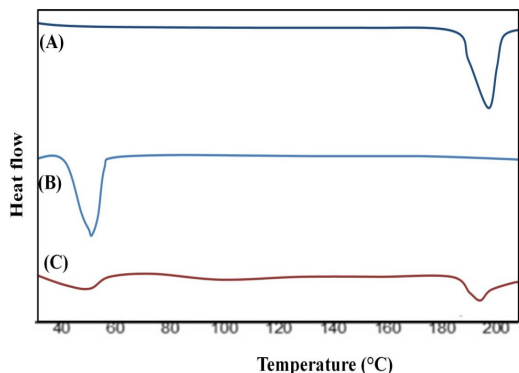


Figure 3: Thermograms of (A) CUR, (B) CSM and (C) CUR-ENPs

### XRD analysis

Figure 4 illustrates the XRD patterns of three key components: CUR, CSM, and the prepared CUR-ENPs (F9). The XRD analysis is crucial for understanding the structural characteristics and changes in the crystallinity of these materials. The XRD pattern of pure CUR displays distinct peaks at various  $2\theta$  angles at  $7.85^\circ$ ,  $8.75^\circ$ ,  $11.87^\circ$ ,  $13.76^\circ$ ,  $14.63^\circ$ ,  $15.62^\circ$ ,  $17.15^\circ$ ,  $19.61^\circ$ , and  $23.72^\circ$ , indicating the crystalline nature of CUR.<sup>14</sup> These sharp peaks signify the regular arrangement of molecules in a crystalline lattice structure, typical of solid-state crystalline materials. The XRD pattern of CSM exhibits peaks at  $2\theta$  angles of  $15.23^\circ$ ,  $17.180^\circ$ , and  $19.82^\circ$ , representing its characteristic crystalline peaks. These peaks confirm the crystalline nature of CSM, providing a reference for its solid-state structure. The XRD pattern of CUR-ENPs showcases reduced peak intensity, and several peaks are either diminished or absent. These changes suggest a notable transition from a crystalline to an amorphous state in the CUR-ENPs.<sup>24</sup> The reduction in peak intensity and disappearance of peaks indicate a disruption in the regular crystalline structure, signifying an enhancement in CUR solubility. The disappearance or reduction of peaks in the XRD pattern of CUR-ENPs indicates that the incorporation of CUR into the polymeric matrix of CSM during the formulation process has disrupted the crystalline lattice structure. The transition from a crystalline to an amorphous state is a positive outcome, as amorphous forms of drugs often exhibit improved solubility, dissolution rates, and bioavailability compared to their crystalline counterparts. The observed alterations in the XRD pattern align with the

bioavailability.

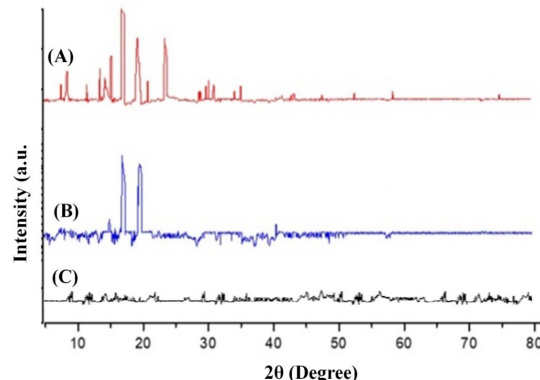


Figure 4: Diffractograms of (A) CUR, (B) CSM and (C) CUR-ENPs

findings from the DSC analysis, collectively confirming the successful transformation of CUR into an amorphous state within the CUR-ENPs. In conclusion, the XRD patterns provide compelling evidence of the transition from crystalline to amorphous states in the prepared CUR-ENPs, reinforcing the potential for enhanced solubility, a critical factor in drug delivery and bioavailability.

### FTIR analysis

Figure 5 presents the spectra of three components: pure CUR, CSM, and the CUR-ENPs (F9). The FTIR spectral analysis allows for the identification of functional groups and provides insights into molecular interactions. The spectrum of CUR exhibits characteristic peaks at specific wavenumbers, such as  $3105.05\text{ cm}^{-1}$  (O-H stretching),  $1674.14\text{ cm}^{-1}$  (C=O-ring),  $1466.24\text{ cm}^{-1}$  (C=C carbonyl stretching),  $1231.68\text{ cm}^{-1}$  (C-O), and  $1375.6\text{ cm}^{-1}$  (C-O-C stretching). These peaks correspond to distinct functional groups in CUR and are indicative of its molecular structure.<sup>14</sup> The spectra of CSM reveal peaks at  $3520.20\text{ cm}^{-1}$  (O-H stretching),  $2912.52\text{ cm}^{-1}$  (C-H stretching),  $1432.66\text{ cm}^{-1}$  (O-H bending), and  $1198.11\text{ cm}^{-1}$  (C-O stretching). These peaks are characteristic of functional groups in CSM and contribute to understanding its molecular composition. The spectra of CUR-ENPs display peaks resembling those of CSM, suggesting the presence of the polymer in the formulation. Simultaneously, alterations in CUR-specific peaks are observed. Deviations in peak patterns in the CUR-ENPs spectra indicate potential intermolecular interactions between CUR and CSM. These interactions contribute to changes in the molecular environment of CUR within the

nanoparticles.<sup>14</sup> The observed alterations in the CUR-ENPs spectra, particularly in the CUR-specific peaks, suggest potential intermolecular interactions between curcumin and CSM. These interactions likely arise from the incorporation of CUR into the polymeric matrix during the formulation of CUR-ENPs. The resemblance of certain peaks in the CUR-ENPs spectra to those of CSM supports the idea that the polymer is a significant component of the formulation. FTIR spectroscopy provides valuable evidence of molecular changes and interactions, aligning with findings from other analyses, such as XRD and

DSC. These complementary techniques collectively confirm the successful encapsulation of CUR in the engineered electro sprayed nanoparticles and suggest changes in the molecular environment of CUR within the electro sprayed nanoformulation. In summary, the spectral analysis in Figure 5 supports the hypothesis of intermolecular interactions between CUR and CSM in the formulated CUR-ENPs, providing valuable insights into the molecular composition and potential changes in the CUR-ENPs formulation.

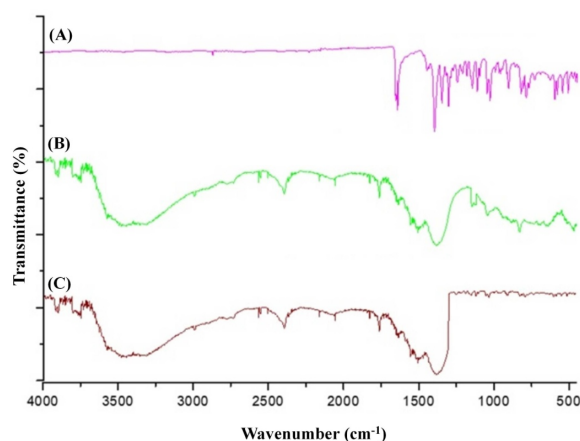


Figure 5: FTIR spectra of (A) CUR, (B) CSM and (C) CUR-ENPs

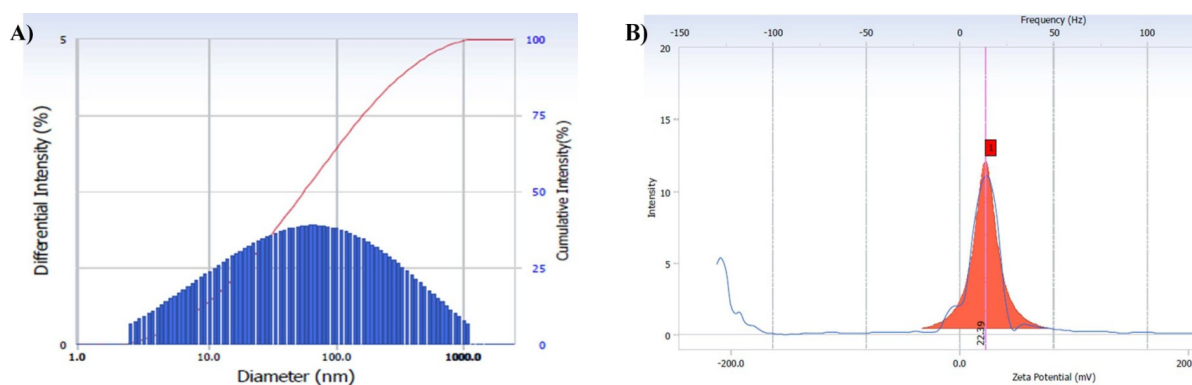


Figure 6: (A) Particle size and (B) zeta potential of CUR-ENPs

### Particle size, PDI and zeta potential analysis

The analysis of the optimized batch (F9) of CUR-ENPs revealed several key characteristics, highlighting the effectiveness of the electro spraying technique in producing stable and nanosized particles. The mean particle size of the optimized CUR-ENPs batch was determined to be approximately 82.2 nm. This value signifies the formation of nanosized particles through the electro spraying process. Nanoparticles in this size range are advantageous for various applications, including drug delivery, as they often exhibit

improved bioavailability and cellular uptake. The PDI was found to be 0.32. A PDI of 0.32 indicates a relatively narrow and uniform size distribution of CUR-ENPs in the solvent system. This uniformity is essential for ensuring consistent performance and behavior of the nanoparticles. The zeta potential of the optimized CUR-ENPs was measured at 22.39 mV. A positive zeta potential of 22.39 mV suggests good stability of the CUR-ENPs in the solvent system. A higher zeta potential often correlates with increased particle stability, as it indicates a

stronger repulsion between particles, minimizing the likelihood of aggregation. The small particle size of 82.2 nm contributes to the increased particulate solubility of CUR-ENPs, a crucial factor for drug delivery applications, as smaller particles often exhibit enhanced dissolution rates.<sup>38</sup> The low PDI indicates a homogeneous size distribution, ensuring consistent performance and behavior of CUR-ENPs. The positive zeta potential further supports the stability of CUR-ENPs in the solvent system, indicating a reduced risk of particle aggregation.<sup>38</sup> The combination of small particle size, low PDI, and positive zeta potential collectively confirms the successful formation of stable and nanosized CUR-ENPs through the electro spraying technique.

### SEM analysis

The SEM analysis of the optimized CUR-ENPs (F9) through the electro spraying technique, as depicted in Figure 7 (A and B), provides valuable insights into the morphology and structure of the nanoparticles. The SEM images reveal that the optimized CUR-ENPs exhibit a particle size within nanosized dimensions, specifically less than 100 nm. The nanosized dimensions are advantageous for drug delivery applications, as smaller particles often contribute to enhanced bioavailability and cellular uptake.

The SEM images depict a smooth surface morphology of the CUR-ENPs with a regular spherical shape. A smooth and regular surface is desirable in nanoparticle formulations, as it can influence aspects, such as stability, drug release kinetics, and interactions with biological systems. The SEM analysis shows no aggregation of CUR-ENPs. The absence of aggregation is a crucial characteristic, as it ensures the uniform distribution of nanoparticles, contributing to consistent performance and behavior. Overall, the SEM analysis serves to verify the successful formation of electro sprayed ENPs encapsulated within the polymeric matrix of CSM. The confirmation of the intended morphology and absence of aggregation aligns with the earlier characterization techniques, reinforcing the overall success of the electro spraying technique in producing the desired nanoparticle structure. Overall, the nanosized dimensions, smooth surface morphology, and absence of aggregation collectively validate the successful fabrication of engineered nanoparticles via the electro spraying technique. These characteristics are crucial for the potential applications of CUR-ENPs in drug delivery, where particle size, morphology, and uniformity significantly affect therapeutic efficacy.

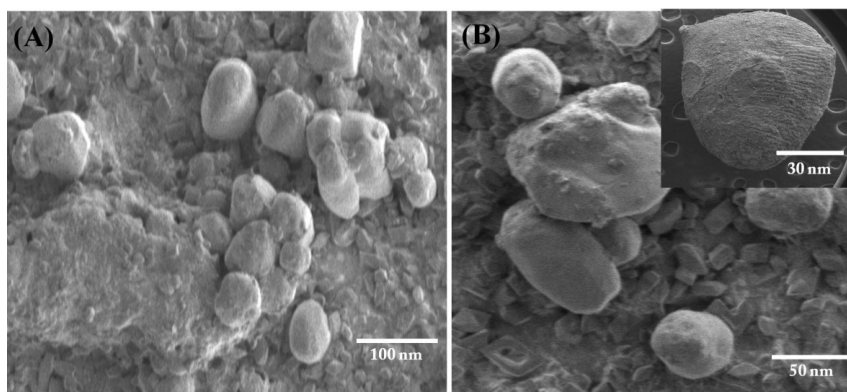


Figure 7: SEM images (A, B) of CUR-ENPs (scale bar: 100 nm, 50 nm, and 30 nm)

### Cell viability analysis

#### *Biocompatibility study on FHC-CRL-1831 cell line*

Cell viability experiments were meticulously conducted on both CUR and CUR-ENPs using the FHC-CRL-1831 normal cell line. The scope of the cytotoxicity investigation spanned a spectrum of CUR concentrations, ranging from 20  $\mu\text{g/mL}$  to 120  $\mu\text{g/mL}$  within the CUR-ENPs formulation. In summary, the outcomes of this

study revealed a direct correlation between the viability of FHC-CRL-1831 cells and the concentration of free CUR. The utilization of dimethyl sulfoxide (DMSO) as a positive control reflected an  $18.55 \pm 2.87\%$  cell viability baseline. Conversely, CUR-ENPs demonstrated minimal cytotoxicity toward FHC-CRL-1831 cells (depicted in Fig. 8A). Notably, no discernible correlation emerged between cytotoxicity and the concentration of CUR within the CSM ENPs.

This observation underscores the superior biocompatibility of CUR-ENPs with colorectal cells compared to bare CUR. The enhanced biocompatibility observed with CUR-ENPs can be attributed to the encapsulation of CUR within the polymeric matrices of CSM. This encapsulation likely contributes to the observed reduction in cytotoxicity. Statistical analysis via single-factor ANOVA confirmed a statistically significant difference ( $p$ -value  $<0.05$ ) in the biocompatibility of CUR-ENPs when juxtaposed with pure CUR.

#### Cell cytotoxicity study on HCT116 cell line

The evaluation of cell cytotoxicity was extended to the HCT116 cell line, shedding light on the comparative effects of bare CUR and CUR-ENPs at varying concentrations. The results, as elucidated in Figure 8B, demonstrate a clear dose-dependent response and affirm the enhanced cytotoxicity of CUR-ENPs compared to bare CUR in the HCT116 cell line. CUR-ENPs exhibited a % cell viability ranging from  $91.03 \pm 1.2\%$  at  $20 \mu\text{g/mL}$  to  $29.22 \pm 1.85\%$  at  $120 \mu\text{g/mL}$  of CUR concentration. The decrease in % cell viability with increasing CUR concentration

illustrates a dose-dependent response, a characteristic often associated with the therapeutic efficacy of drug formulations. In contrast, bare CUR displayed a % cell viability ranging from  $98.22\%$  to  $52.12\%$  for CUR concentrations spanning  $20 \mu\text{g/mL}$  to  $120 \mu\text{g/mL}$ . The stark contrast between CUR-ENPs and bare CUR % cell viability affirms the superior performance of CUR-ENPs in cell viability in the HCT116 cell line. The higher % cell viability reduction observed with CUR-ENPs underscores their superior cancer cell cytotoxicity in comparison to bare CUR. These findings suggest that CUR-ENPs showed more cytotoxicity to cancer cells of HCT116. The results reinforce the potential of CUR-ENPs as a promising option for applications involving colorectal cancer cell lines, highlighting their ability to mitigate cytotoxic effects while delivering CUR. In conclusion, the dose-dependent response of CUR-ENPs in the HCT116 cell line, as opposed to bare CUR, underscores the enhanced potential efficacy of CUR-ENPs. These findings position CUR-ENPs as a promising candidate for further exploration and development in the context of colorectal cancer treatment.

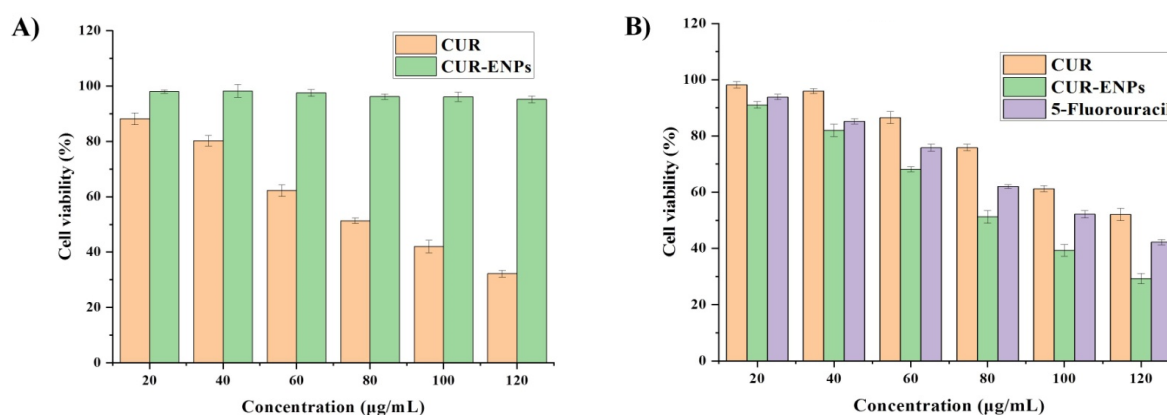


Figure 8: Cell viability study of CUR and CUR-ENPs on FHC-CRL-1831 cells and HCT116 cell line

#### CONCLUSION

The present study introduces the formulation of CUR-ENPs, composed of CUR and CSM, using the electrospraying technique to enhance the solubility of poorly soluble CUR. Successfully prepared, the CUR-ENP formulations were optimized using the  $3^2$  (three-level, two-factor) response surface methodology. Analysis through DSC and XRD confirmed the reduction in CUR crystallinity, signifying improved solubility due to probable intermolecular interactions between CUR and CSM, resulting in the formation of nanosized

particles. SEM analysis validated the formation of spherical CUR-ENPs, while zeta potential analysis confirmed their excellent stability. Notably, the customized release of up to 12 h was achieved, owing to the preference for CSM. In phosphate buffer (pH 7.4) fluids, CUR-ENPs released 85.45% to 94.25% of their loading within 12 h, a stark contrast to pure CUR, which released only 42.85% in 12 h. Cell line studies on normal intestinal cells attested to the superior biocompatibility of CUR-ENPs compared to bare CUR. Additionally, the observed reduction in cell viability of colorectal cancer cells confirmed the

promising anticancer potential of CUR-ENPs over bare CUR. In conclusion, the application of electrospraying technology presents a notable advancement in solubility, modified release, biocompatibility, and enhanced anticancer potential. Considering its low cost, simplicity, and eco-friendly nature, the electrospraying technique stands as a favorable approach for designing polymer nanoparticles loaded with poorly soluble phytoconstituents and synthetic drug molecules in future applications.

**ACKNOWLEDGMENT:** The authors are thankful to the principal of R. C. Patel Institute of Pharmaceutical Education and Research, Shirpur, for providing the necessary facilities to carry out the project effectively.

## REFERENCES

- P. Rawla, T. Sunkara and A. Barsouk, *Prz. Gastroenterol.*, **14**, 89 (2019), <https://doi.org/10.5114/pg.2018.81072>
- Z. Li, X. Shan, Z. Chen, N. Gao, W. Zeng *et al.*, *Adv. Sci.*, **8**, 2002589 (2021), <https://doi.org/10.1002/adv.202002589>
- M. Cuffy, F. Abir, R. A. Audisio and W. E. Longo, *Surg. Oncol.*, **13**, 149 (2004), <https://doi.org/https://doi.org/10.1016/j.suronc.2004.08.002>
- X. Gu, Y. Wei, Q. Fan, H. Sun, R. Cheng *et al.*, *J. Control. Release.*, **301**, 110 (2019), <https://doi.org/10.1016/j.jconrel.2019.03.005>
- C. J. Punt, M. Koopman and L. Vermeulen, *Nat. Rev. Clin. Oncol.*, **14**, 235 (2017), <https://doi.org/10.1038/nrclinonc.2016.171>
- V. Gyanani, J. C. Haley and R. Goswami, *Pharmaceuticals*, **14**, 835 (2021), <https://doi.org/10.3390/ph14090835>
- S. Das, K. K. Ciombor, S. Haraldsdottir and R. M. Goldberg, *Curr. Treat. Options Oncol.*, **19**, 29 (2018), <https://doi.org/10.1007/s11864-018-0543-z>
- H. Xiao, L. Yan, E. M. Dempsey, W. Song, R. Qi *et al.*, *Prog. Polym. Sci.*, **87**, 70 (2018), <https://doi.org/10.1016/j.progpolymsci.2018.07.004>
- C. Eng, *Nat. Rev. Clin. Oncol.*, **6**, 207 (2009), <https://doi.org/10.1038/nrclinonc.2009.16>
- P. Parashar, C. B. Tripathi, M. Arya, J. Kanoujia, M. Singh *et al.*, *Phytomedicine*, **53**, 107 (2019), <https://doi.org/10.1016/j.phymed.2018.09.013>
- M. Rizwanullah, S. Amin, S. R. Mir, K. U. Fakhri and M. M. A. Rizvi, *J. Drug Target.*, **26**, 731 (2018), <https://doi.org/10.1080/1061186X.2017.1408115>
- M. Mahdian, S. A. Asrari, M. Ahmadi, T. Madrakian, N. R. Jalal *et al.*, *J. Drug Deliv. Sci. Technol.*, **84**, 104537 (2023), <https://doi.org/10.1016/j.jddst.2023.104537>
- W.-Y. Wang, Y.-X. Cao, X. Zhou and B. Wei, *Drug Des. Dev. Ther.*, 2205 (2019), <https://doi.org/10.2147/DDDT.S205787>
- U. Patil, S. Rawal, J. Pantwalawalkar, S. Nangare, D. Dagade *et al.*, *Thai J. Pharm. Sci.*, **46**, 711 (2023), <https://digital.car.chula.ac.th/tjps/vol46/iss6/11>
- J. Y. Yu, J. A. Kim, H. J. Joung, J. A. Ko and H. J. Park, *J. Food Sci.*, **85**, 3866 (2020), <https://doi.org/10.1111/1750-3841.15489>
- Y. Zhang, A. Rauf Khan, M. Fu, Y. Zhai, J. Ji *et al.*, *J. Drug Target.*, **27**, 917 (2019), <https://doi.org/10.1080/1061186X.2019.1572158>
- C. Enrico, *Stud. Nat. Prod. Chem.*, **62**, 91 (2019), <https://doi.org/10.1080/1061186X.2019.1572158>
- M. Zamani, M. P. Prabhakaran and S. Ramakrishna, *Int. J. Nanomed.*, **8**, 2997 (2013), <https://doi.org/10.2147/IJN.S43575>
- R. Sridhar and S. Ramakrishna, *Biomatter*, **3**, e24281 (2013), <https://doi.org/10.4161/biom.24281>
- S. Malik, S. Subramanian, T. Hussain, A. Nazir and S. Ramakrishna, *Curr. Pharm. Des.*, **28**, 368 (2022), <https://doi.org/10.2174/1381612827666210929114621>
- J. Varshosaz, E. Ghassami, A. Noorbakhsh, A. Jahanian-Najafabadi, M. Minaiyan *et al.*, *Drug Dev. Ind. Pharm.*, **44**, 1012 (2018), <https://doi.org/10.1080/03639045.2018.1430819>
- X. Luo, G. Jia, H. Song, C. Liu, G. Wu *et al.*, *Pharm. Res.*, **31**, 46 (2014), <https://doi.org/10.1007/s11095-013-1130-4>
- Y. Başpınar, H. Akbaba and O. Bayraktar, *J. Res. Pharm.*, **23**, 886 (2019), <https://doi.org/10.35333/jrp.2019.36>
- E. Sayed, C. Karavasili, K. Ruparelia, R. Haj-Ahmad, G. Charalambopoulou *et al.*, *J. Control. Release.*, **278**, 142 (2018), <https://doi.org/10.1016/j.jconrel.2018.03.031>
- H. Yu, Y. Wang, S. Wang, X. Li, W. Li *et al.*, *ACS Appl. Mater. Interfaces*, **10**, 43462 (2018), <https://doi.org/10.1021/acsami.8b16487>
- S. Y. Lee, J.-J. Lee, J.-H. Park, J.-Y. Lee, S.-H. Ko *et al.*, *Colloids Surf. B Biointerf.*, **145**, 267 (2016), <https://doi.org/10.1016/j.colsurfb.2016.05.009>
- M. Dick, T. M. H. Costa, A. Goma, M. Subirade, A. de Oliveira Rios *et al.*, *Carbohydr. Polym.*, **130**, 198 (2015), <https://doi.org/10.1016/j.carbpol.2015.05.040>
- V. Y. Ixtaina, S. M. Nolasco and M. C. Tomás, *Ind. Crop. Prod.*, **28**, 286 (2008), <https://doi.org/10.1016/j.indcrop.2008.03.009>
- B. Singh, G. Chauhan, S. Kumar and N. Chauhan, *Carbohydr. Polym.*, **67**, 190 (2007), <https://doi.org/10.1016/j.carbpol.2006.05.006>
- K.-Y. Lin, J. R. Daniel and R. L. Whistler, *Carbohydr. Polym.*, **23**, 13 (1994), [https://doi.org/10.1016/0144-8617\(94\)90085-X](https://doi.org/10.1016/0144-8617(94)90085-X)
- L. Munoz, J. Aguilera, L. Rodriguez-Turienzo, A. Cobos and O. Diaz, *J. Food Eng.*, **111**, 511 (2012), <https://doi.org/10.1016/j.jfoodeng.2012.02.031>

- <sup>32</sup> L. Brüttsch, F. J. Stringer, S. Kuster, E. J. Windhab and P. Fischer, *Food Funct.*, **10**, 4854 (2019), <https://doi.org/10.1039/C8FO00173A>
- <sup>33</sup> M. S. Hosseini and M. R. Nabid, *Int. J. Biol. Macromol.*, **163**, 336 (2020), <https://doi.org/10.1016/j.ijbiomac.2020.06.252>
- <sup>34</sup> H. Xu, J. Jaynes and X. Ding, *Stat. Sin.*, **24**, 269 (2014), <https://doi.org/10.5705/ss.2012.210>
- <sup>35</sup> C. Human, D. De Beer, M. Van Der Rijst, M. Aucamp and E. Joubert, *Food Chem.*, **276**, 467 (2019), <https://doi.org/10.1016/j.foodchem.2018.10.016>
- <sup>36</sup> A. A. K. Zarchi, S. Abbasi, M. A. Faramarzi, K. Gilani, M. Ghazi-Khansari *et al.*, *Int. J. Biol. Macromol.*, **72**, 764 (2015), <https://doi.org/10.1016/j.ijbiomac.2014.09.004>
- <sup>37</sup> R. Sun, C. Shen, S. Shafique, O. Mustapha, T. Hussain *et al.*, *Int. J. Nanomed.*, **15**, 705 (2020), <https://doi.org/10.2147/IJN.S235146>
- <sup>38</sup> T. Powar, A. Hajare, R. Jarag and S. Nangare, *Acta Chim. Slov.*, **68**, 861 (2021), <https://doi.org/10.17344/acsi.2021.6858>
- <sup>39</sup> S. Nangare, S. Dugam, P. Patil, R. Tade and N. Jadhav, *Nanotechnology*, **32**, 035101 (2020), <https://doi.org/10.1088/1361-6528/abb8a9>
- <sup>40</sup> L. A. Raj, R. Jonisha, B. Revathi and E. Jayalakshmy, *J. Appl. Pharm. Sci.*, **5**, 001 (2015), <https://doi.org/10.7324/JAPS.2015.50701>
- <sup>41</sup> D. Ghadge, S. Nangare and N. Jadhav, *J. Drug Deliv. Sci. Technol.*, **72**, 103354 (2022), <https://doi.org/10.1016/j.jddst.2022.103354>
- <sup>42</sup> S. S. Patel, H. A. Pushpadass, M. E. E. Franklin, S. N. Battula and P. Vellingiri, *J. Food Sci. Technol.*, **59**, 1326 (2022), <https://link.springer.com/doi/10.1007/s13197-021-05142-0>